

Effect of doping on electronic states in B-doped polycrystalline CVD diamond films

This article has been downloaded from IOPscience. Please scroll down to see the full text article.

2012 Semicond. Sci. Technol. 27 065019

(<http://iopscience.iop.org/0268-1242/27/6/065019>)

View [the table of contents for this issue](#), or go to the [journal homepage](#) for more

Download details:

IP Address: 137.222.43.33

The article was downloaded on 28/05/2012 at 12:20

Please note that [terms and conditions apply](#).

Effect of doping on electronic states in B-doped polycrystalline CVD diamond films

O S Elsherif^{1,4}, K D Vernon-Parry¹, J H Evans-Freeman² and P W May³

¹ Materials and Engineering Research Institute, Sheffield Hallam University, Sheffield S1 1WB, UK

² College of Engineering, University of Canterbury, Christchurch, New Zealand

³ School of Chemistry, University of Bristol, Bristol BS8 1TS, UK

E-mail: osama.s.el-sherif@student.shu.ac.uk

Received 7 November 2011, in final form 20 April 2012

Published 21 May 2012

Online at stacks.iop.org/SST/27/065019

Abstract

High-resolution Laplace deep-level transient spectroscopy (LDLTS) and thermal admittance spectroscopy (TAS) have been used to determine the effect of boron (B) concentration on the electronic states in polycrystalline chemical vapour deposition diamond thin films grown on silicon by the hot filament method. A combination of high-resolution LDLTS and direct-capture cross-sectional measurements was used to investigate whether the deep electronic states present in the layers originated from point or extended defects. There was good agreement between data on deep electronic levels obtained from DLTS and TAS experiments. Two hole traps, E1 (0.29 eV) and E2 (0.53 eV), were found in a film with a boron content of $1 \times 10^{19} \text{ cm}^{-3}$. Both these levels and an additional level, E3 (0.35 eV), were found when the B content was increased to $4 \times 10^{19} \text{ cm}^{-3}$. Direct capture cross-sectional measurements of levels E1 and E2 show an unusual dependence on the fill-pulse duration which is interpreted as possibly indicating that the levels are part of an extended defect. The E3 level found in the more highly doped film consisted of two closely spaced levels, both of which show point-like defect characteristics. The E1 level may be due to B-related extended defects within the grain boundaries, whereas the ionization energy of the E2 level is in agreement with literature values from *ab initio* calculations for B–H complexes. We suggest that the E3 level is due to isolated B-related centres in bulk diamond.

(Some figures may appear in colour only in the online journal)

1. Introduction

It is becoming clear that silicon-based power devices cannot achieve the varied and demanding requirements and design goals set by industry because the theoretical limits of silicon are being approached as Si technology advances. Wide band gap semiconductors such as gallium nitride and diamond are likely to be candidates to replace silicon in power applications in the future. Thin-film diamond has become a very attractive material because it provides an extraordinary combination of optical, thermal and electrical properties, due to its very strong sp^3 bonding [1] and excellent resilience to harsh environments,

which makes it a material that has potential in many advanced applications; it has significantly better figures of merit than any other material. However, the electronic properties of chemical vapour deposition (CVD) diamond are affected by defects and impurities introduced both during the growth and subsequent processing steps during device fabrication. Although impressive results have already been demonstrated [2, 3], a lot of processing issues still need to be analysed and significant development work remains to be carried out before semiconducting diamond can seriously challenge the existing technologies.

Diamond has a very wide band gap, widely reported as being about 5.5 eV; most natural diamonds are insulators, and thus doping by electrically active impurities such as boron

⁴ Author to whom any correspondence should be addressed.

or phosphorus is required to turn thin diamond films into p- or n-type semiconductors. Boron is known as the most effective acceptor in diamond if it is to be used in electronic devices [4]. The dopant ionization energies, especially in polycrystalline diamond, are higher than ideal, at about 0.36–0.37 eV [4–6], meaning that the full ionization of the dopant at room temperature is unlikely to be achieved. A gradual change from a semiconducting to metallic state and then to a superconducting state is observed as the boron doping level increases from 10^{18} to above $4 \times 10^{20} \text{ cm}^{-3}$ [7]. However, it is also known that more than 10% of the boron atoms incorporated into diamond do not act as acceptors [8, 9]. Some may be electrically inactive; it has been suggested that some boron atoms are passivated by due to their association with other impurities such as hydrogen [9], although annealing schedules can reduce the concentration of these complexes. It is also a possibility that boron may segregate into highly defective regions of the material which could result in complexes of B with vacancies and boron interstitial defects [10, 11]. In polycrystalline diamond films, B may also segregate to the grain boundaries and be trapped there as inert impurities.

Semiconducting diamond can be grown by a variety of CVD methods (hot filament, microwave plasmas or direct current glow discharge) [12–14]; some of the properties of the diamond films produced, such as the crystallite size, the nature of the grain boundaries, the hydrogen content and the defect density, may differ according to the CVD method used.

One of the major problems with polycrystalline diamond films is a tendency for them to contain high defect densities due to their non-homogeneous structure and abundance of grain boundaries. Monocrystalline diamond overcomes these problems, but large-scale production is still thought to be largely impracticable due to growth requirements and fairly low growth rates of high pressure–high temperature diamond which limits the monocrystal size to volumes of about 1 cm^3 . Therefore, heteroepitaxial CVD of polycrystalline diamond films on Si substrates remains the industrial growth method of choice for many devices. High-quality polycrystalline diamond films have recently been reported [15, 16], with grains that range in size from micrometres to less than 5 nm.

It has been reported [17] that hole mobility for B-doped polycrystalline diamond can be improved by increasing the grain size and that such material can exhibit much better field-effect transistor properties than single-crystal material. The mechanisms underpinning these findings are still not clear; this underscores the ongoing requirement for a deeper and more thorough understanding of the physics of defects in polycrystalline diamond.

Capacitance deep level transient spectroscopy (DLTS) [18] has been a powerful technique for investigating the electronic behaviour of deep levels in semiconductors for decades. DLTS experiments can yield information about both electron and hole traps in a material, can be used to determine the density and capture the cross-section of individual defect levels, and can also distinguish between point and extended defects. A high-resolution modification of DLTS, LDLTS [19], records the capacitance transient due to carrier emission from

a trap at a fixed temperature and extracts all the emission rates present in the transient by applying different mathematical algorithms. The LDLTS software offers a library of algorithms which are either modified for the requirements of LDLTS or developed specifically for this system [20–22]. The three different algorithms (CONTIN, FTIKREG and FLOG) used are based on the Tikhonov regularization method, and they differ only in the way the regularization parameters are defined. Use of more than one algorithm provides a comparative analysis of the emission rate, increasing confidence in the accuracy of the generated LDLTS spectra. LDLTS is capable of distinguishing whether a single DLTS peak is due to emission from a unique defect or several defects closely spaced in energy. The choice of measurement temperature is usually (but not necessarily) governed by the original DLTS measurement, i.e. an optimum temperature is chosen for each deep state, which is around the maximum of the DLTS peak.

Thermal admittance spectroscopy (TAS) is a slightly less sensitive technique than DLTS [18] as the deep-level response is probed only by a small region and not by the whole space-charge region as in the standard DLTS technique. However, electric field effects on the ionization energy are more easily controlled with the admittance method [23]. Although a mode of DLTS can be employed that ensures field consistency, the method is more difficult to control than TAS; hence, the use of the latter technique in this report.

Over the last two decades various activation energies and capture cross-sections have been reported for majority carrier traps in semiconducting diamond using capacitance transient spectroscopy techniques such as DLTS. [24–26] However, some of these data may have been misinterpreted due to the low resolution of the experimental measurements. Recently valuable information about defects in monocrystalline [27, 28] and polycrystalline [3, 29] diamond films have been obtained; however, the precise origin of these traps has still not been confirmed.

In this work, a comparison of electrically active defects in polycrystalline CVD diamond with different boron levels was carried out. We have applied the high-resolution Laplace DLTS technique to establish whether the traps detected by DLTS are due to single- or multiple-carrier emissions, and direct capture cross-sectional measurements have been used to demonstrate whether the detected deep electronic states originated from point or extended defects. Finally, results from TAS and DLTS have been compared for semiconducting diamond.

2. Experimental details

Boron-doped polycrystalline diamond films were deposited on heavily boron-doped Si substrates by hot filament CVD (HFCVD). The gas mixture used was high purity H_2 (200 sccm), CH_4 (2 sccm) and diborane (B_2H_6) as a variable source of boron. These gases were metred into the chamber via mass flow controllers with the process pressure maintained at 20 Torr. Rhenium was used for the filament material since Re does not act as a sink for carbon or boron species. The estimated filament temperature was $\sim 2000^\circ \text{C}$ and the estimated Si surface temperature (combined heat from

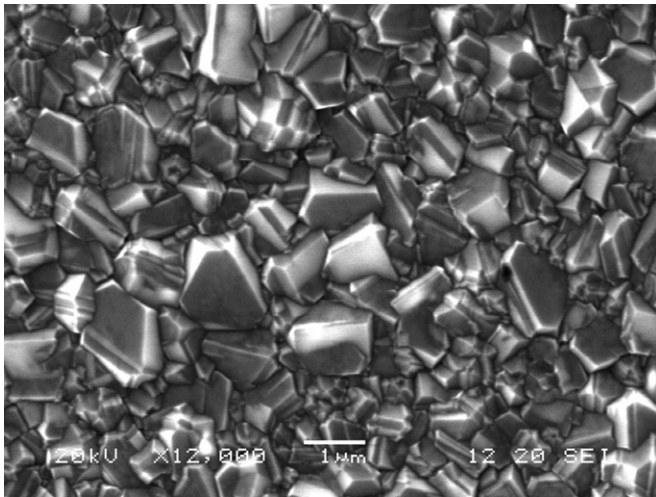


Figure 1. Electron micrograph of a CVD boron-doped diamond film, scale is shown for 1 μm .

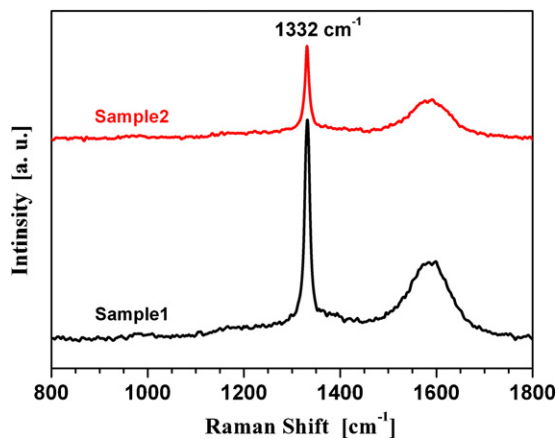


Figure 2. Raman spectra for the different boron-doped microcrystalline diamond films 1 and 2, using UV (325 nm) excitation. The spectra have been offset vertically from each other for clarity.

filament and substrate heater) was $\sim 900^\circ\text{C}$. The single-crystal (100) Si substrates (p+, resistivity 0.01–0.02 $\Omega\text{ cm}$) were manually abraded before deposition using 1–3 μm diamond grit, to facilitate the diamond nucleation.

The growth time was 8 h, producing polycrystalline films of thickness $\sim 3\ \mu\text{m}$. Figure 1 shows a typical scanning electron microscope image of a CVD boron-doped diamond film; the film morphology was microcrystalline with faceted crystallites averaging $\sim 1\ \mu\text{m}$ in size. The quality of the diamond films was verified by Raman spectroscopy, and the Raman spectra of samples 1 and 2 confirmed the presence of polycrystalline diamond in both films as illustrated in figure 2, presenting a sharp peak centred at $1332\ \text{cm}^{-1}$, corresponding to the sp^3 -bonded structure [30].

An estimation of the B content was made for each film by comparison with a calibration graph of four-point probe resistivity measurements against B-content measured by SIMS [30]. This procedure gives the total B content in the film, which is likely to be higher than the concentration of electrically active B due to compensation or segregation, as mentioned

earlier. The B concentration in these samples was estimated to be $1.5 \times 10^{19}\ \text{cm}^{-3}$ in sample 1 and $4 \times 10^{19}\ \text{cm}^{-3}$ in sample 2, which means that they could be considered ‘medium’ doped and semiconducting, rather than metallic. The diamond films were degreased using trichloroethylene followed by acetone; the samples were then immersed in a saturated solution of H_2SO_4 and HNO_3 acid at around 200°C for 20 min to remove any graphitic layers and to O-terminate the surface. The films were subsequently annealed in vacuum at 750°C for 30 min. Schottky contacts (1 mm diameter dots) were formed on the oxidized diamond surface with Al deposited by thermal evaporation through a patterned mask; there were approximately eight Schottky devices on each $0.5 \times 0.5\ \text{cm}^2$ sample. Al Ohmic contacts were evaporated on the Si back surface.

Prior to DLTS experiments, capacitance–voltage (C – V) and current–voltage (I – V) measurements were performed to check the integrity of the diodes, and also to obtain information about current transport mechanisms across the junction. The rectifying characteristics and the Schottky barrier heights were investigated for the Al contacts. Saturation current (I_0) values were obtained by extrapolating the linear region of the semi-logarithmic forward I – V curves to zero voltage and then were used to calculate the apparent barrier height (Φ_b). The ideality factor (n) was calculated from the slope of the linear region of the semi-logarithmic forward I – V characteristics. The I – V characteristics of the diodes (up to eight diodes on each film) were recorded using a Keithley 6487 picoammeter.

DLTS on the Schottky diode was carried out using a range of fill-pulse voltages. LDLTS was then carried out at fixed temperatures in a high stability cryostat; several thousand capacitance transients were averaged, which ensured that the signal-to-noise ratio was of the order of 1000, which was enough to separate transients with closely spaced emission rates. The LDLTS transient was analysed by three different inverse Laplace transform algorithms, and a plot of peak intensity as a function of emission rate produced. A combination of LDLTS and direct capture cross-sectional measurements was used to demonstrate whether the electrically active defects present in the material are due to point or extended defects.

Thermal admittance spectroscopy measurements were performed between 80 and 450 K with the samples in a closed-cycle He high-stability cryostat at a vacuum level of 10^{-6} Torr. Measurements were performed using an Agilent E4980A LCR metre. The experiments were carried out with an ac test signal of 100 mV and probing frequencies of 1, 50, 250 kHz and 1 MHz during sample cool down.

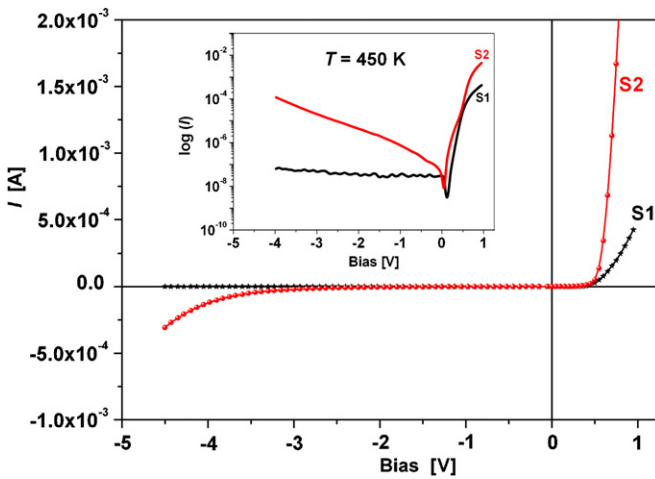
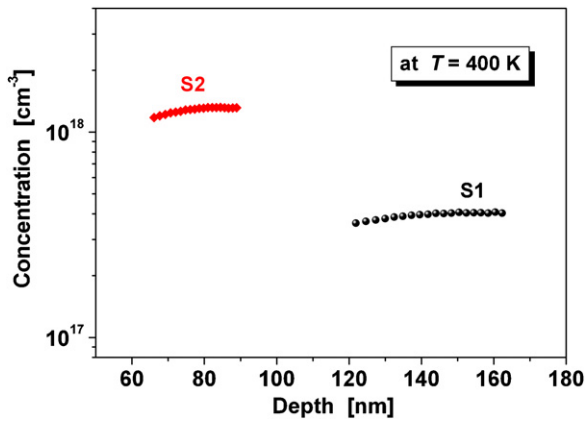
3. Results and discussion

3.1. The I – V and C – V measurements

Figure 3 shows the I – V characteristics for diodes on both films at 450 K; the inset shows the $\log(I)$ versus V plot. Table 1 details the Schottky diode properties for both diodes in the temperature range of 200–450 K. The zero-bias barrier height decreased with decreasing temperature ($\sim 1\ \text{eV}$ at 300 K).

Table 1. Schottky diode parameters for samples 1 and 2 measured by I - V and C - V plots.

T (K)	Sample 1				Sample 2			
	n	R_s (I_V) (Ω)	$\Phi_{b(I_V)}$ (eV)	$\Phi_{b(C_V)}$ (eV)	n	R_s (I_V) (Ω)	$\Phi_{b(I_V)}$ (eV)	$\Phi_{b(C_V)}$ (eV)
200	2.2	2360	0.83	2.36	3.6	1203	0.66	1.95
250	1.94	1866	0.94	2.38	3.2	729	0.79	2.05
300	1.8	1590	1.17	2.25	2.9	638	0.95	2.30
350	1.7	1444	1.25	2.18	2.5	401	1.12	2.24
400	1.4	1242	1.37	2.1	2.3	327	1.17	2.15
450	1.2	980	1.48	1.95	2.1	294	1.26	2.03

**Figure 3.** The I - V characteristics for diodes fabricated on samples 1 (S1) and 2 (S2) at 450 K. The inset shows the $\log(I)$ versus V plot.**Figure 4.** The C - V concentration–depth profiles obtained for Schottky diodes in samples 1 (S1) and 2 (S2).

Schottky barrier heights between ~ 0.8 and 2.2 eV have been reported in the literature [31–34]; our measured value of the barrier height is within this range. Recent theoretical studies [35] have revealed barrier heights of 1.1 eV for Al contacts on H-terminated diamond.

An example of C - V data at 400 K is plotted in figure 4, revealing the profile of carrier concentrations within the space-charge region of a Schottky diode on each of the samples. As expected, the doping was found to be uniform in the space-charge regions investigated. C - V measurements were also carried out at lower temperatures at which there was less complete ionization and the data inserted into the DLTS

analysis. The carrier concentration was higher in sample 2 and the depletion region was narrower (~ 25 nm) than in sample 1 (~ 45 nm), again as expected. However, carrier concentrations were much lower than the estimated boron-doping density in both samples; confirmation that in these layers a large population of the boron atoms incorporated into diamond are not acting as acceptors [8, 9].

From the C - V data, the built-in potential (V_{bi}) values were deduced from the extrapolation of $1/C^2$ to zero, and the Schottky barrier heights ($\Phi_{b(C_V)}$) were calculated from these values at 300 – 450 K. These data are listed in table 1. It is reported by Nebel *et al* [36] that the barrier height of Al on B-doped diamond, evaluated using C - V measurements, is 1.95 eV; this agrees very well with the value obtained for sample 1.

Variations of the barrier height over the contact area can occur as a result of non-uniformity of the interfacial layer thickness, inhomogeneities in the interfacial layer composition, and/or distributions of interfacial charges. The variations in the ideality factor with temperature are related to barrier inhomogeneities and also to the degree of its deformation under the applied bias. The evolution of the ideality factor and relevant barrier inhomogeneities has been widely discussed by other authors [37, 38].

3.2. The DLTS and LDLTS measurements

DLTS experiments were performed at 1 MHz with six rate windows (RWs) and different biasing conditions. Figures 5(a) and (b) show the DLTS spectra for samples 1 and 2, respectively, performed with RWs 20 s $^{-1}$ and 50 s $^{-1}$, respectively, at a reverse bias of -3 V and fill pulse of -0.5 V applied for 50 ms.

The DLTS spectra for sample 1 revealed two majority carrier traps. The first peak (E1) was around 170 K with an activation energy of 0.29 ± 0.03 eV and the second peak (E2) covered a wide range of temperatures from 320 to 440 K with an activation energy of 0.53 ± 0.07 eV. These activation energies were extrapolated from the Arrhenius plot shown in figure 6. Both peaks shift towards higher temperatures for higher RWs as expected. However, the peaks are asymmetric with a tail on the low-temperature side (and was almost the same for all RWs), a feature which can be typical of an extended defect in some materials [39]. However, this should not be treated as a strong indication of such type of defect.

The high-temperature peak (E2) observed may contain multiple emissions as it covers a wide range of temperatures

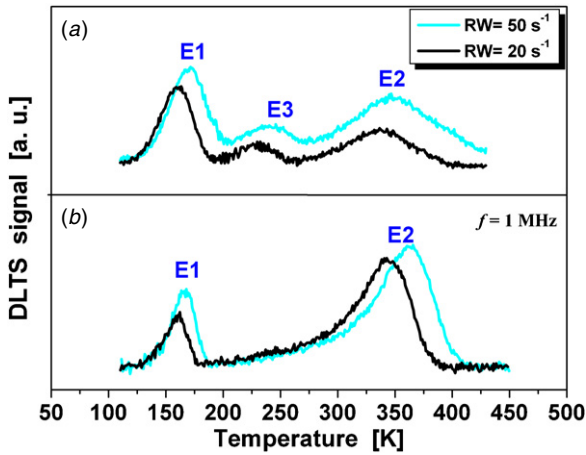


Figure 5. DLTS spectra of (a) sample 1 and (b) sample 2, with rate windows (RWs) 20 and 50 s⁻¹, reverse bias of -3 V, fill pulse of -0.5 V and the measurement frequency of 1 MHz.

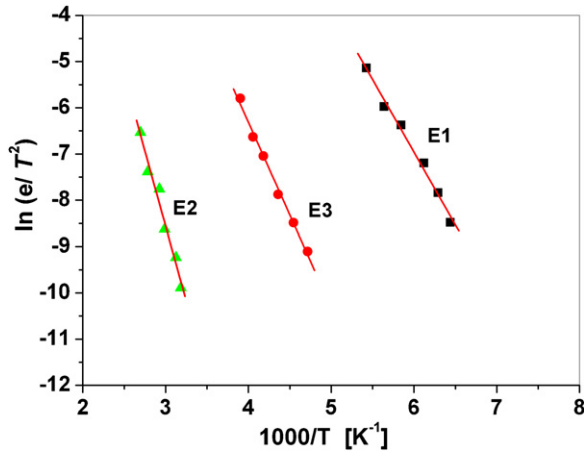


Figure 6. Arrhenius plot, derived from the DLTS spectra.

in both samples. Kiyota *et al* [24] reported a trap level with an activation energy of 0.6 eV above the valence band edge in boron-doped polycrystalline diamond films grown on Si substrates using HFCVD. They argued that the detected level is either generated by the hot filament technique applied to grow this diamond or is related to grain boundaries in the polycrystalline diamond. Alternatively, Lombardi [11] has calculated the properties of boron and its complexes with hydrogen in diamond using DFT methods; his results show that BH₂ centres are stable with small binding energies of 0.23–0.71 eV. It can be argued that it is very likely that hydrogen is present in larger volumes near the interface because the annealing has removed H nearer the surface, giving rise to this level. Kumar *et al* [40] have theoretically investigated the BH and BH₂ complexes in B-doped diamond. They predicted the associated acceptor levels to be $E_v + 4.44$ eV and $E_v + 1.14$ eV, respectively. The associated donor levels were found to be $E_c - 4.84$ eV and $E_c - 2.80$ eV, respectively. The BH donor level at $E_c - 4.84$ eV (corresponding to $E_v + 0.6$ eV) is found to be at the same energy level as the donor level of the vacancy [41]. These are in good agreement with recent results measured by isothermal transient spectroscopy [28]. The atomic structure of the complex defect BH₃ is less well

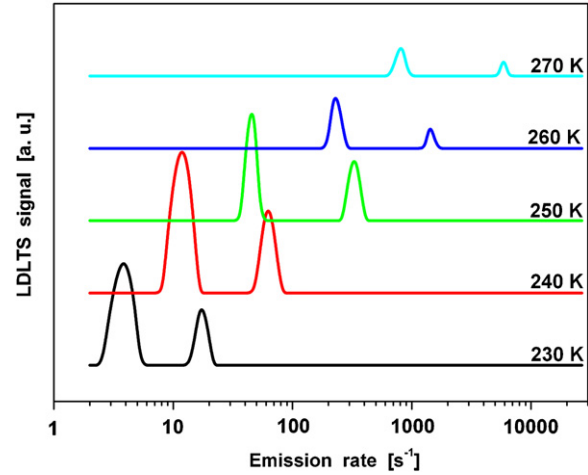


Figure 7. LDLTS of sample 2 at temperatures 230–270 K with a reverse bias of -3 V, fill pulse of -0.5 V and fill pulse length of 50 ms.

understood; it is predicted to form a donor level at $E_v + 0.20$ eV [10]. Recently, Muret *et al* [28, 42] have reported that hole traps with ionization energies between 0.7 and 1.6 eV are most likely due to hydrogen-related defects. Further details about deep donor levels and deep acceptor levels related to boron, hydrogen, or structural defects in B-doped diamond calculated by the *ab initio* method and attribution to traps observed by DLTS is given in [28].

The DLTS spectra of sample 2 (figure 5(b)) show that a new majority carrier trap (E3) was detected centred around 250 K, with an activation energy of 0.35 ± 0.07 eV, trap density (N_T) $\sim 3 \times 10^{16}$ cm⁻³. A defect with a similar activation energy has been reported in B-doped diamond, grown by HFCVD, detected by TAS in the 170–270 K temperature range [43].

In order to verify the nature of the DLTS features, LDLTS measurements were performed under the same biasing conditions as DLTS, over the entire temperature range that the DLTS feature spanned.

LDLTS measurements were carried out on E1 in samples 1 and 2 at a range of temperatures (not shown). The carrier emission rates did not change with temperature, and it is likely that this is because we were unable to sample for long enough due to very slow emission rates, particularly at the low temperatures. Therefore, although one could speculate that this might indicate the electronic levels giving rise to the emission are not pure point defects, these data would need considerable further investigation. A detailed capture cross-sectional measurement which also indicates that extended defects could be contributing to these spectra is discussed next.

Figure 7 shows the LDLTS results for sample 2 at temperatures around the peak maximum of the DLTS peak E3. Results have demonstrated the presence of two closely spaced defects, the emission rates of which vary with temperature in a consistent manner throughout the entire range 230–270 K, behaviour typical of point-like defects. Therefore, activation-energy calculations were possible for these levels; the activation energy of the defect appearing at lower emission

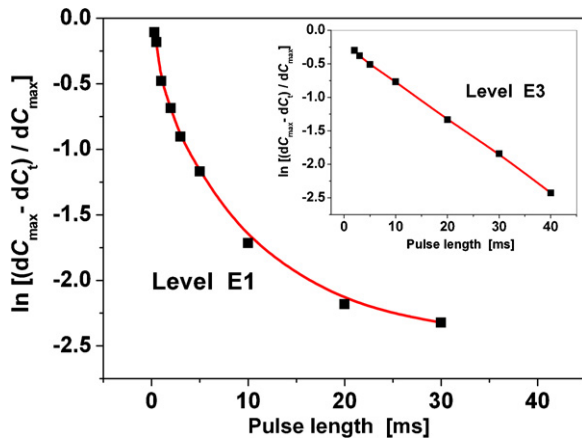


Figure 8. The capacitance change as a function of the fill-pulse length of the defect at E1 in sample 1 (■) and the defect at E3 in sample 2 (*); a reverse bias of -3 V and a fill pulse of -0.5 V were applied to the samples. For E1, the data were recorded at 170 K, whereas for E3 the data were recorded at 250 K.

rate was found to be 0.35 eV, while the activation energy of the higher emission rate defect was 0.37 eV. This is in very good agreement with the result from the less sensitive DLTS Arrhenius plot of the single feature in figure 5(b). We suggest that these defects responsible for E3 are B-related point defects situated in the bulk of the films.

It is well known that extrapolated capture cross-sections from Arrhenius plots can have uncertainties of several orders of magnitude and need to be treated with caution. There are various reasons for this discrepancy: a small overlapping effect with a neighbouring signal in DLTS and the fact that DLTS relies on the emission-rate changes induced by temperature. It has been proven that electric-field-enhanced emission tends to generate errors in cross-sections [44, 45]. A more reliable technique for determining the capture properties is by using various pulse widths at a fixed temperature [19, 45] where the capture time can be determined by varying t_p and hence carrier emission does not affect the results.

Figure 8 shows the capacitance change as a function of the fill-pulse length for defects E1 in sample 1 (at 170 K) and E3 in sample 2 (at 250 K), at a reverse bias of -3 V and a fill pulse of -0.5 V, in accordance with equation (1) [18]:

$$\ln \left[\frac{\Delta C_\infty - \Delta C_t}{\Delta C_\infty} \right] = \sigma_p \cdot v_{th} \cdot p \cdot t_p, \quad (1)$$

where ΔC_∞ is the equilibrium capacitance value, ΔC_t is the capacitance at time t , σ_p is the trap capture cross-section, p is the majority carrier population, t_p is the fill-pulse duration and v_{th} is the thermal velocity.

The majority capture cross-section should obey a linear dependence on the logarithm of a combination of capacitance terms as a function of pulse length. This provides a sensitive test for the presence of isolated point defects only if the mobile holes concentration is instantaneously provided to a level where holes could be captured by the deep centres. Deviation from this relationship may provide a test for the presence of extended defects. However, the causes of nonlinearity in the capture cross-sectional data could be explained by different scenarios. The first scenario could be that, equation (1) is not

valid for E1, as the hole emission time for the transition from the ground state to delocalized states in the valence band falls into the fill-pulse time range. For example, if one assumes shallow acceptors like in single-crystalline diamond, with a capture cross-section of 4×10^{-13} cm² and $E_a = 0.37$ eV (at 170 K), the emission time is estimated to be 3 ms [46]. This reduces the likelihood of the mobile holes concentration to be instantaneously available to be captured by the deep centres and resulting in a nonlinear characteristic. Such a limitation disappears at 200 K and above. Therefore, E1 could be due to point-like defects.

The second scenario could be that the level E1 is grain-boundary-related states. This is a reasonable suggestion since it has been only reported in polycrystalline diamond [47–49], although this has not been proven. In this case, the trap distribution will be very inhomogeneous and the defects may be sufficiently closely spaced that the presence of a filled trap will reduce the likelihood of a neighbouring empty trap capturing a hole. Therefore, E1 could be due to an extended defect exhibiting Coulombic repulsion, because the repulsive force reduces subsequent carrier capture at the defect which is slowly charging up.

In the case of E2, the ionization should be fast enough, as this trap is emitting at $T > 200$ K. However, nonlinearity is observed in the capture cross-sectional data for samples 1 and 2 (recorded at 360 K); hence, equation (1) does not hold. It has been reported in [42], for B-doped monocrystalline diamond that the origin of the majority carrier traps located in energy between the top of the valence band and circa 1.6 eV is related to hydrogen, confirming previous predictions [40, 42]. Based on these findings, one can suggest that E2 may be due to the BH donor level.

The defect at E3 in sample 2 was also examined at 250 K under similar biasing conditions. The recorded data show excellent linearity when plotted in accordance with equation (1), as shown in figure 8, and hence it was possible to extract the capture cross-section by calculating the gradient of the graph; it was found to be 3×10^{-15} cm².

It has been reported [39, 50] that the DLTS signal should exhibit a dependence on the logarithm of the fill-pulse time when the carrier capture is into extended defects,

$$\Delta C_m \propto \ln(t_p), \quad (2)$$

where ΔC_m denotes the amplitude of the DLTS signal.

Figure 9 shows the data for levels E1 and E2 in sample 1 plotted in accordance with equation (2). An excellent fit was obtained, thus demonstrating that the defects giving rise to this capture characteristic may be extended-defect-like states.

3.3. Thermal admittance spectroscopy measurements

Figure 10 shows TAS spectra recorded at $f_T = 1, 50, 250$ kHz and 1 MHz for sample 2 at a reverse bias of -3 V; the inset shows a TAS spectrum for sample 1 at 50 kHz, where G is the measured conductance and f_T is the probing frequency. Both samples were cooled down in the (450–100) K temperature range.

It is worth mentioning that TAS and DLTS experiments were carried out using two different setups but under similar

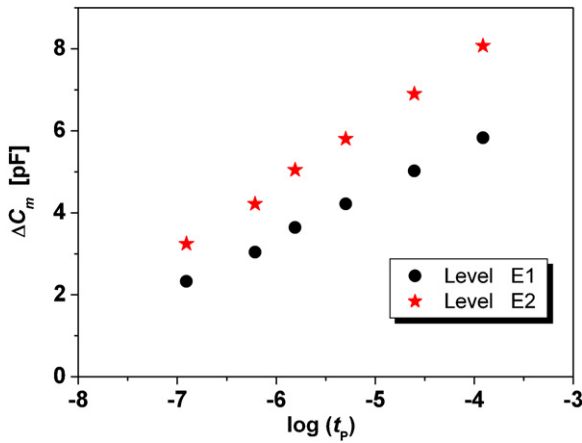


Figure 9. DLTS signal as a function of the logarithm of the filling time for the defect at E1 (■) and the defect at E2 (●) in sample 1, measured at 170 and 360 K, respectively. The reverse bias was set at -3 V and a fill pulse of -0.5 V.

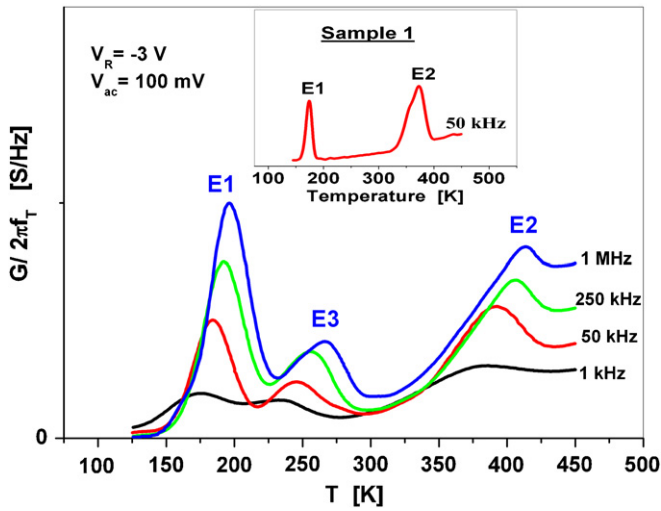


Figure 10. Experimental curves of conductance G divided by $\omega = 2\pi f_T$ as a function of temperature for sample 2; the reverse bias was -3 V and the probing frequencies were $f_T = 1, 50, 250$ kHz and 1 MHz. The inset shows a G/w plot for sample 1, recorded at $V_R = -3$ V and $f_T = 50$ kHz.

vacuum conditions $\sim 10^{-4}$ Pa. In all experiments, the data were recorded using a temperature scan rate of 4 K min^{-1} . A dependence of the G/ω peak position (figure 10), and the corresponding capacitance step (figure 11), on the probing frequency f_T and/or sample temperature is observed. The G/ω versus T data qualitatively reproduce the behaviour observed in the DLTS experiments, and the activation energies of the trap levels determined by TAS agree fairly well with those calculated from DLTS. Two hole traps E1 (0.26 ± 0.04) and E2 (0.58 ± 0.03) were detected in the G/ω versus T spectra of samples 1 and 2, and an additional level E3 (0.36 ± 0.02) was observed only in sample 2. The peaks shift towards higher temperatures with increasing probing frequency, indicating an increase in hole-emission rate. It is possible to directly use the conductance peaks occurring at each temperature to construct an Arrhenius plot, and hence the acceptor activation energy

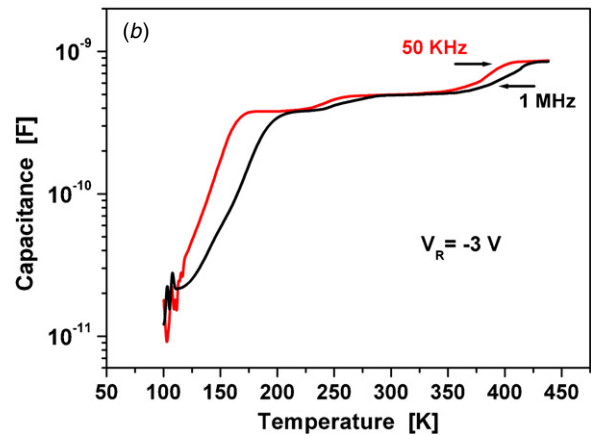
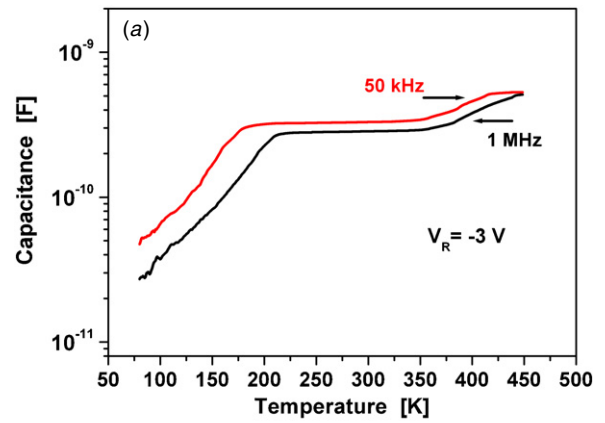


Figure 11. Capacitance–temperature plots of (a) sample 1 and (b) sample 2, recorded with frequencies 50 kHz and 1 MHz, at a reverse bias of -3 V.

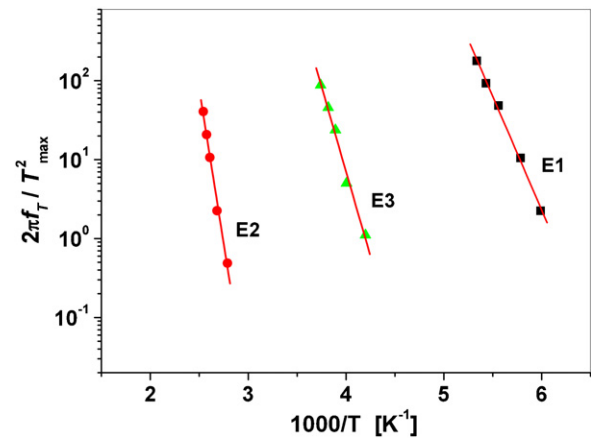


Figure 12. Arrhenius plot, derived from the TAS spectra.

and the apparent capture cross-section (σ_p) of each defect can be deduced according to the standard equation [51]:

$$\frac{2\pi f_T}{T_{\max}^2} = \gamma \cdot \sigma_p \cdot \exp\left(\frac{-E_a}{kT_{\max}}\right), \quad (3)$$

$$\gamma = \sqrt{96\pi^3} \cdot g \cdot \frac{m^* \cdot k^2}{h^3}, \quad (4)$$

where E_a is the trap activation energy, T_{\max} is the temperature of the conductance peak, m^* is the effective mass of the hole, h is Planck's constant, k is the Boltzmann constant and g is

Table 2. Summary of the deep levels calculated by DLTS and admittance spectroscopy.

Trap	N_T^a (cm ⁻³)	$E_T - E_V$ (eV)		σ_p (cm ²)	
		DLTS	TAS	DLTS	TAS ^b
E1	5×10^{16}	0.29 ± 0.03	0.26 ± 0.04	n/a ^c	2×10^{-18}
E2	7×10^{16}	0.53 ± 0.07	0.58 ± 0.03	n/a ^c	8×10^{-19}
E3	3×10^{16}	0.35 ± 0.02	0.36 ± 0.02	3×10^{-15}	2×10^{-15}

^a Trap concentration calculated from DLTS.

^b Measured at 0 V.

^c Accurate values cannot be determined by DLTS because equation (1) does not have a linear fit.

the degeneracy factor. A least-squares fitting procedure gives a straight line, the slope of which corresponds to the trap activation energy, as shown in figure 12. The capture cross sections of all three traps were deduced from the intercept with the vertical axis. As illustrated in table 2, TAS offers capture cross-section extrapolation (at zero reverse bias and 100 mV ac signal) for traps associated with extended defects (E1 and E2). Capture cross-sectional calculations for E1 and E2 were not possible using the DLTS data because equation (1) was not valid (did not have a linear fit). It should be noted again that electric field effects on the ionization energy are well controlled in TAS [18].

4. Conclusions

Deep trap levels in boron-doped diamond have been investigated experimentally using DLTS, high-resolution LDLS and TAS, as a function of doping concentration. Data recorded by DLTS and TAS yielded identical information about the deep levels in CVD-diamond films; these were identified by DLTS as hole traps. TAS and DLTS have been compared for semiconducting diamond.

LDLS experiments confirmed that two trap levels, closely spaced in energy, have been introduced in the more highly doped film (sample 2); their emission rates changed consistently with temperature and the activation energies were found to be close to that of substitutional B (0.36 eV). These two levels appeared in DLTS and TAS as a single feature (E3), which we have discussed in terms of B-related centres in bulk diamond.

The capture characteristics and filling of the observed deep levels have been investigated in detail by varying the duration of the filling pulse in high-resolution DLTS experiments. The capacitance change was fitted to a linear dependence on the natural logarithm of the fill-pulse duration. The DLTS signal at levels E1 and E2 exhibited linear dependence on the logarithm of the fill-pulse time, which may be indicative of carriers being trapped at a large electrically active defect, demonstrating that the trapping may be in defects in the strain field of an extended defect. The electrical behaviour of the defects E3 did not exhibit linear dependence on the logarithm of the fill-pulse time; therefore we conclude that this trap contains only isolated point defects, which is consistent with it being associated with B-related centres in bulk diamond.

References

- [1] Kalish R 2007 *J. Phys. D: Appl. Phys.* **40** 6467
- [2] May P W, Ludlow W J, Hannaway M, Smith J A, Rosser K N and Heard P J 2008 *Mater. Res. Soc. Symp. Proc.* p 1039
- [3] Polyakov V I, Rukovichnikov A I, Avdeeva L A, Kun'kova Z E, Varnin V P, Teremetskaya I G and Ralchenko V G 2006 *Diam. Relat. Mater.* **15** 1972–5
- [4] Kalish R 1999 *Carbon* **37** 781
- [5] Tomio O and Tadashi S 2004 *Diam. Relat. Mater.* **13** 2037–40
- [6] Yamanaka S, Takeuchi D, Watanabe H, Okushi H and Kajimura K 1999 *Phys. Status Solidi a* **174** 59
- [7] Rashid S J et al 2006 *Diam. Relat. Mater.* **15** 317–23
- [8] Gabrysch M, Majdi S, Hallén A, Linnarsson M, Schner A, Twitchen D and Isberg J 2008 *Phys. Status Solidi a* **205** 2190
- [9] Chevallier J, Theys B, Lusson A, Gratepain C, Deneuville A and Gheeraert E 1998 *Phys. Rev. B* **58** 7966
- [10] Goss J P, Briddon P R, Sque S J and Jones R 2004 *Phys. Rev. B* **69** 165215
- [11] Lombardi E B 2009 *Diam. Relat. Mater.* **18** 835–8
- [12] May P W 2000 *Phil. Trans. R. Soc. Lond. A* **358** 473–95
- [13] Lindlbauer A, Haubner R and Lux B 1992 *Wear* **159** 67–77
- [14] Ferreira I, Costa M E V, Pereira L, Fortunato E, Martins R, Ramos A R and Silva M F 2001 *Appl. Surf. Sci.* **184** 8–19
- [15] Wang L, Chen X, Wu G, Guo W, Cao S, Shang K and Han W 2011 *Thin Solid Films* **520** 752–5
- [16] May P W and Mankelevich Y A 2008 *J. Phys. Chem. C* **112** 12432–41
- [17] Hiram K, Takayanagi H, Yamauchi S, Yang J H, Kawarada H and Umezawa H 2008 *Appl. Phys. Lett.* **92** 112107
- [18] Lang D V 1974 *J. Appl. Phys.* **45** 3023
- [19] Dobaczewski L, Kaczor P, Hawkins I D and Peaker A R 1994 *J. Appl. Phys.* **76** 194
- [20] Provencher S W 1982 *Comput. Phys. Commun.* **27** 213
- [21] Weese J 1992 *Comput. Phys. Commun.* **69** 99
- [22] Matulis A FLOG developed for LDLS *Copernicus Project CIPA CT-94 0172*
- [23] Pautrat J L, Katircioglu B, Magnea N, Bensahel D, Pfister J C and Revoil L 1980 *Solid-State Electron.* **23** 1159
- [24] Kiyota H, Okushi H, Okano K, Akiba Y, Kurosu T and Iida M 1992 *Appl. Phys. Lett.* **61** 1808
- [25] Zeisel R, Nebel C E and Stutzmann M 1998 *J. Appl. Phys.* **84** 6105
- [26] Gaudin O, Troupis D K, Jackman R B, Nebel C E and Gheeraert E 2003 *J. Appl. Phys.* **94** 5832
- [27] Tavares C, Muret P, Koizumi S and Jomard F 2007 *Phys. Status Solidi a* **204** 2985
- [28] Muret P, Pernot J, Kumar A, Magaud L, Mer-Calfati C and Bergonzo P 2010 *Phys. Rev. B* **81** 235205
- [29] Thurzo I, Zahn D R T and Dua A K 2001 *Semicond. Sci. Technol.* **16** 527–33
- [30] May P W, Ludlow W J, Hannaway M, Heard P J, Smith J A and Rosser K N 2008 *Diam. Relat. Mater.* **17** 105–17

- [31] Takeuchi D, Yamanaka S, Watanabe H, Okushi H and Kajimura K 2000 *Appl. Surf. Sci.* **159** 572
- [32] Yamanaka S, Watanabe H, Masai S, Kawata S, Hayashi K, Okushi H and Kajimura K 1998 *J. Appl. Phys.* **84** 6095
- [33] Evans D A, Roberts O R, Williams G T, Vearey-Roberts A R, Bain F, Evans S, Langstaff D and Twitchen D J 2009 *J. Phys.: Condens. Matter.* **21** 364223
- [34] Evans D A, Roberts O R, Vearey-Roberts A R, Langstaff D P, Twitchen D J and Schwitters M 2007 *Appl. Phys. Lett.* **91** 132114
- [35] Kageshima H and Kasu M 2009 *Japan. J. Appl. Phys.* **48** 111602
- [36] Nebel C E, Zeisel R and Stutzmann M 1999 *Phys. Status Solidi a* **174** 117
- [37] Werner J H and Guttler H H 1991 *J. Appl. Phys.* **69** 1522–33
- [38] Aboelfotoh M O, Cros A, Svensson B G and Tu K N 1990 *Phys. Rev. B* **41** 9819–27
- [39] Grillot P N, Ringel S A, Fitzgerald E A, Watson G P and Xie Y H 1995 *J. Appl. Phys.* **77** 3248
- [40] Kumar A, Pernot J, Deneuville A and Magaud L 2008 *Phys. Rev. B* **78** 235114
- [41] Jones R 2009 *Diam. Relat. Mater.* **18** 820
- [42] Muret P, Volpe P-N, Pernot J and Omnès F 2011 *Diam. Relat. Mater.* **20** 722–52
- [43] Chiquito A J, Berengue Olívia M, Diagonel E, Galzerani José C and Moro João R 2007 *J. Appl. Phys.* **101** 033714
- [44] Wang A C and Sah C T 1985 *J. Appl. Phys.* **57** 4645
- [45] Schroder D K 2006 *Semiconductor Material and Device Characterization* (New York: Wiley)
- [46] Glesener J W 1994 *Appl. Phys. Lett.* **64** 217
- [47] Polyakov V I, Rukovichnikov A I, Varnin V P, Teremetskaya I G and Laptev V A 2003 *Diam. Relat. Mater.* **12** 1783–7
- [48] Gaudin O, Whitfield M D, Foord J S and Jackman R B 2001 *Diam. Relat. Mater.* **10** 610–14
- [49] Mitromara N, Evans-Freeman J H, Gädtke C and May P W 2008 *Phys. Status Solidi a* **205** 2184–9
- [50] Figielski T 1978 *Solid-State Electron.* **21** 1403
- [51] Blood P and Orton J W 1992 *The Electrical Characterization of Semiconductors: Majority Carriers and Electrons States* (San Diego, CA: Academic)